An Adaptive Control Technology for Safety of a GTM-like Aircraft

Megumi Matsutani
Massachusetts Institute of Technology, Cambridge, Massachusetts

Luis G. Crespo
National Institute of Aerospace, Hampton, Virginnia

Anuradha Annaswamy and Jinho Jang
Massachusetts Institute of Technology, Cambridge, Massachusetts

NASA STI Program . . . in Profile

Since its founding, NASA has been dedicated to the advancement of aeronautics and space science. The NASA scientific and technical information (STI) program plays a key part in helping NASA maintain this important role.

The NASA STI program operates under the auspices of the Agency Chief Information Officer. It collects, organizes, provides for archiving, and disseminates NASA's STI. The NASA STI program provides access to the NASA Aeronautics and Space Database and its public interface, the NASA Technical Report Server, thus providing one of the largest collections of aeronautical and space science STI in the world. Results are published in both non-NASA channels and by NASA in the NASA STI Report Series, which includes the following report types:

- TECHNICAL PUBLICATION. Reports of completed research or a major significant phase of research that present the results of NASA programs and include extensive data or theoretical analysis. Includes compilations of significant scientific and technical data and information deemed to be of continuing reference value. NASA counterpart of peer-reviewed formal professional papers, but having less stringent limitations on manuscript length and extent of graphic presentations.

- TECHNICAL MEMORANDUM. Scientific and technical findings that are preliminary or of specialized interest, e.g., quick release reports, working papers, and bibliographies that contain minimal annotation. Does not contain extensive analysis.

- CONTRACTOR REPORT. Scientific and technical findings by NASA-sponsored contractors and grantees.

- CONFERENCE PUBLICATION. Collected papers from scientific and technical conferences, symposia, seminars, or other meetings sponsored or co-sponsored by NASA.

- SPECIAL PUBLICATION. Scientific, technical, or historical information from NASA programs, projects, and missions, often concerned with subjects having substantial public interest.

- TECHNICAL TRANSLATION. English-language translations of foreign scientific and technical material pertinent to NASA's mission.

Specialized services also include creating custom thesauri, building customized databases, and organizing and publishing research results.

For more information about the NASA STI program, see the following:

- Access the NASA STI program home page at *http://www.sti.nasa.gov*

- E-mail your question via the Internet to help@sti.nasa.gov

- Fax your question to the NASA STI Help Desk at 443-757-5803

- Phone the NASA STI Help Desk at 443-757-5802

- Write to:
  NASA STI Help Desk
  NASA Center for AeroSpace Information
  7115 Standard Drive
  Hanover, MD 21076-1320

An Adaptive Control Technology for Safety of a GTM-like Aircraft

Megumi Matsutani
Massachusetts Institute of Technology, Cambridge, Massachusetts

Luis G. Crespo
National Institute of Aerospace, Hampton, Virginnia

Anuradha Annaswamy and Jinho Jang
Massachusetts Institute of Technology, Cambridge, Massachusetts

Abstract

An adaptive control architecture for safe performance of a transport aircraft subject to various adverse conditions is proposed and verified in this report. This architecture combines a nominal controller based on a Linear Quadratic Regulator (LQR) with integral action, and an adaptive controller that accommodates actuator saturation and bounded disturbances. The effectiveness of the baseline controller and its adaptive augmentation are evaluated and compared using a stand-alone control verification methodology. Case studies that pair individual parameter uncertainties with critical flight maneuvers are studied. The resilience of the controllers is determined by evaluating the degradation in closed-loop performance resulting from increasingly larger deviations in the uncertain parameters. Symmetric and asymmetric actuator failures, flight upsets, and center of gravity displacements, are some of the uncertainties considered.

Nomenclature

b_{ref}	wingspan
c_{ref}	mean aerodynamic chord
C_L	Aerodynamic force coefficient in the minus z-direction of the wind axes
C_D	Aerodynamic force coefficient in the minus x-direction of the wind axes
C_Y	Aerodynamic force coefficient in the minus y-direction of the wind axes
C_l	Aerodynamic moment coefficient in the x-direction of the body axes
C_m	Aerodynamic moment coefficient in the y-direction of the body axes
C_n	Aerodynamic moment coefficient in the z-direction of the body axes
C_{xy}	Partial derivative of C_x with respect to y
d	Design variable
e	State error
f	Flight maneuver
$\mathcal{F}$	Failure domain
g	Constraint function
h	Altitude
I_{ab}	Component of the inertia tensor in the ab direction
L	Aerodynamic torque in the in the x-direction of the body axes
M	Aerodynamic torque in the in the y-direction of the body axes
$\mathcal{M}$	Maximal set
N	Aerodynamic torque in the in the z-direction of the body axes
p	Uncertain parameter
$\bar{p}$	Nominal parameter point
$\tilde{p}$	Critical parameter value
u_n	Baseline control

u_a	Adaptive control
U_0	Control value for trim
u	Component of the velocity relative to the air in the x-direction of the body axes
v	Component of the velocity relative to the air in the y-direction of the body axes
w	Component of the velocity relative to the air in the z-direction of the body axes
W	Vehicle's weight
x	state vector of the plant
x_m	state vector of the reference model
X	Aerodynamic force in the in the x-direction of the body axes
Y	Aerodynamic force in the in the y-direction of the body axes
Z	Aerodynamic force in the in the z-direction of the body axes
$\tilde{\alpha}$	Critical similitude ratio
Δ_x	CG position in the x-direction of the body axes relative to a reference point
Δ_y	CG position in the y-direction of the body axes relative to a reference point
Δ_z	CG position in the z-direction of the body axes relative to a reference point
Λ	Control effectiveness matrix
ρ	Parametric safety margin

Acronyms

CG	Center of gravity
CPV	Critical parameter Value
CSR	Critical Similitude Ratio
DOF	Degrees of fredom
FC	Flight Condition
GTM	Generic Transport Model
LQR	Linear Quadratic Regulator
MS	Maximal Set
PSM	Parametric Safety Margin

1   Introduction

The challenge of achieving safe flight comes into sharp focus in the face of adverse conditions caused by faults, damage, or upsets. When these situations occur, the corresponding uncertainties directly affect the safe operation of the aircraft. A technology that has the potential for enabling safe flight under these adverse conditions is adaptive control. One of the main features of an adaptive control architecture is its ability to react to changing characteristics of the underlying aircraft dynamics. This paper proposes the building blocks of an adaptive and reconfigurable control technology that ensures safe flight

under adverse flight conditions. This technology enables synthesis of such controllers as well as systematic evaluation of their robustness characteristics.

The field of adaptive control is a mature theoretical discipline that has evolved over the past fifty years, embodying methodologies for controlling uncertain dynamic systems with parametric uncertainties [1]- [2]. Through the efforts of various researchers over this period, systematic methods for the control of linear and nonlinear dynamic systems with parametric and dynamic uncertainties have been developed [3]- [4]. Stability and robustness properties of these systems in the presence of disturbances, time-varying parameters, unmodeled dynamics, time-delays, and various nonlinearities, have been outlined in the references [1]- [5] as well as in several journal and conference papers over the same period.

In this paper, we consider the control of a transport aircraft model that resembles the Generic Transport Model [6]. While the vehicle's geometry and aerodynamic model are those of a C5 aircraft [9], every other aspect has been made similar to the GTM, e.g. anti wind-up logic, time-delay due to telemetry, baseline control structure, low-pass and wash-out filters. We delineate the underlying nonlinear model of this aircraft, and introduce various types of damages, and failures into this model. An adaptive control architecture is proposed which combines a nominal controller that provides a satisfactory performance in the absence of adverse conditions, and an adaptive controller that is capable of accommodating various adverse conditions including actuator saturation. The specific adverse conditions considered can be grouped into the following three categories, (a) upsets, (b) damages, and (c) actuator failures. Specific cases in (a) include flight upsets in initial conditions of various states including angle of attack, cases in (b) include situations where structural failures cause changes in the location of the Center-of-Gravity (CG) [7], while cases in (c) include situations where symmetric and asymmetric failures in control surfaces and engines occur. These failures include loss in control effectiveness, and locked-in-place control surfaces.

The resilience of the adaptive controller to uncertainty is evaluated for safety using the control verification methodology proposed in [8]. This methodology enables the determination of ranges of uncertainty for which a prescribed set of closed-loop requirements are satisfied. This paper studies several one-dimensional uncertainty analyses for two flight maneuvers that focus on the longitudinal and lateral dynamics. As compared to the baseline controller, the adaptive controller enlarges the region of safe operation by a sizable margin in all but one of the cases considered.

3

2 The GTM-Like Aircraft

In this section, we begin with a description of a nonlinear dynamic model of C5, a large transport aircraft whose aerodynamics data is available in [9]. We consider rigid body dynamics, aerodynamics, effect of the control inputs, and derive the overall nonlinear flight model. We then discuss adverse conditions such as flight upsets, damage, and failures, and how to model them.

2.1 Nonlinear Dynamic Model

A typical dynamic model of an aircraft consists of the equations of motion, aerodynamics, actuator dynamics, actuator saturation, and sensor dynamics. The standard conservation equations [10] describe the dynamics of u, v, and w, the body-fixed aircraft velocities; p, q, and r, the roll, pitch, and yaw rates; and the Euler angles ϕ, θ, and ψ. The aircraft's flat-Earth equations of motion are given by

$$\dot{u} = g\frac{X}{W} - g\sin\theta - qw + rv, \tag{1}$$

$$\dot{v} = g\frac{Y}{W} + g\cos\theta\sin\phi - ru + pw, \tag{2}$$

$$\dot{w} = g\frac{Z}{W} + g\cos\theta\cos\phi + qu - pv, \tag{3}$$

$$\dot{p} = \frac{I_{zz}}{I_D}\left[L + I_{xz}pq - (I_{zz} - I_{yy})qr\right] + \frac{I_{xz}}{I_D}\left[N - I_{xz}qr - (I_{yy} - I_{xx})pq\right], \tag{4}$$

$$\dot{q} = \frac{1}{I_{yy}}\left[M - (I_{xx} - I_{zz})pr - I_{xz}\left(p^2 - r^2\right)\right], \tag{5}$$

$$\dot{r} = \frac{I_{xz}}{I_D}\left[L + I_{xz}pq - (I_{zz} - I_{yy})qr\right] + \frac{I_{xx}}{I_D}\left[N - I_{xz}qr - (I_{yy} - I_{xx})pq\right], \tag{6}$$

$$\dot{\phi} = p + q\sin\phi\tan\theta + r\cos\phi\tan\theta, \tag{7}$$

$$\dot{\theta} = q\cos\phi - r\sin\phi, \tag{8}$$

$$\dot{\psi} = (q\sin\phi + r\cos\phi)\sec\theta, \tag{9}$$

In the above, $I_D = I_{xx}I_{zz} - I_{xz}^2$; X, Y, and Z are the aerodynamic forces in body axes at the actual center of gravity (CG), and L, M, and N are the aerodynamic moments about the same point. See the Nomenclature section and Table 1 for the meaning of other symbols. The values of the gross aircraft weight W, the moments of inertia I_{xx}, I_{yy}, and I_{zz}, as well as the product of inertia I_{xz} can be found in [9].

4

The following navigation equations determine x and y, the positions of the aircraft in the north and east directions respectively, as well as the altitude h:

$$\dot{x} = u\cos\theta\cos\psi + v(-\cos\phi\sin\psi + \sin\phi\sin\theta\cos\psi) + \tag{10}$$
$$w(\sin\phi\sin\psi + \cos\phi\sin\theta\cos\psi),$$
$$\dot{y} = u\cos\theta\sin\psi + v(\cos\phi\cos\psi + \sin\phi\sin\theta\sin\psi) + \tag{11}$$
$$w(-\sin\phi\cos\psi + \cos\phi\sin\theta\sin\psi),$$
$$\dot{h} = u\sin\theta - v\sin\phi\cos\theta - w\cos\phi\cos\theta. \tag{12}$$

It is often convenient to replace the body-fixed velocities with the true airspeed V_T, the angle-of-attack α, and the side-slip angle β. These new states can be calculated from the body-fixed velocities, neglecting wind and gust-induced effects, as

$$V_T = \sqrt{u^2 + v^2 + w^2}, \tag{13}$$
$$\tan\alpha = \frac{w}{u}, \tag{14}$$
$$\sin\beta = \frac{v}{V_T}. \tag{15}$$

It is well known [11] that the aerodynamic forces and moments acting on the aircraft can be expressed in terms of the non-dimensional force and moment coefficients through multiplication by a dimensional factor and, in the case of the forces, a transformation from wind to body axes. The forces and moments are therefore given by

$$\begin{bmatrix} X \\ Y \\ Z \end{bmatrix} = \bar{q}S \begin{bmatrix} \cos\alpha & 0 & -\sin\alpha \\ 0 & 1 & 0 \\ \sin\alpha & 0 & \cos\alpha \end{bmatrix} \begin{bmatrix} -C_D\cos\beta \\ C_Y \\ -C_L \end{bmatrix}, \tag{16}$$

$$\begin{bmatrix} L \\ M \\ N \end{bmatrix} = \bar{q}S \begin{bmatrix} b_{ref}C_l \\ c_{ref}C_m \\ b_{ref}C_n \end{bmatrix}, \tag{17}$$

where C_L, C_D, and C_Y are the lift, drag, and side-force coefficients respectively while C_l, C_m, and C_n are the moment coefficients. The values of the wingspan b_{ref}, the mean aerodynamic chord c_{ref}, and the wing surface area S can be found in [9].

Table 1 shows the aircraft states, plant (i.e., inputs to the plant), control (i.e., outputs of the controller), and pilot inputs. The system state vector given by

$$x = \begin{bmatrix} V_T & \alpha & \beta & p & q & r & \phi & \theta & \psi & x & y & h \end{bmatrix}^T. \tag{18}$$

The pilot inputs are commands to ailerons, rudders, and elevators. The plant inputs are the 4 engine throttles and the deflections of 6 control surfaces (i.e.,

Table 1. Aircraft states, actuators, and pilot inputs.

Variable	Description	Component of
V_t	Velocity	State (x)
α	Angle of Attack	State (x)
β	Side-slip Angle	State (x)
ϕ	Euler Angle	State (x)
θ	Euler Angle	State (x)
ψ	Euler Angle	State (x)
p	Roll Rate	State (x)
q	Pitch Rate	State (x)
r	Yaw Rate	State (x)
t_1	Left outboard Throttle	Plant input
t_2	Left Inboard Throttle	Plant input
t_3	Right Inboard Throttle	Plant input
t_4	Right outboard Throttle	Plant input
e_1	Left Elevator	Plant input, Control output (u)
e_2	Right Elevator	Plant input, Control output (u)
a_1	Left Aileron	Plant input, Control output (u)
a_2	Right Aileron	Plant input, Control output (u)
r_1	Lower Rudder	Plant input, Control output (u)
r_2	Upper Rudder	Plant input, Control output (u)
$\delta_{e,cmd}$	Virtual Elevator	Pilot input (r)
$\delta_{a,cmd}$	Virtual Aileron	Pilot input (r)
$\delta_{r,cmd}$	Virtual Rudder	Pilot input (r)

two for elevators, ailerons and rudders). As in the current version of the GTM the engines are not used for control and the throttle values will be fixed at their trim values.

The inputs available to the pilot are the elevator, aileron, and rudder commands denoted as $\Delta\delta_{e,cmd}$, $\Delta\delta_{a,cmd}$, and $\Delta\delta_{r,cmd}$. The aerodynamic force and moment coefficients are given by

$$
\begin{aligned}
C_L &= C_{L_\alpha}\alpha + C_{L_{\delta_e}}\delta_e, \\
C_D &= C_{D_\alpha}\alpha + C_{D_{\delta_e}}\delta_e, \\
C_Y &= C_{Y_\beta}\beta + C_{Y_p}p\frac{b_{ref}}{2V_T} + C_{Y_r}r\frac{b_{ref}}{2V_T} + C_{Y_{\dot\beta}}\dot\beta\frac{b_{ref}}{2V_T} + C_{Y_{\delta_a}}\delta_a + C_{Y_{\delta_r}}\delta_r,
\end{aligned}
\tag{19}
$$

$$
\begin{aligned}
C_l &= C_{l_\beta}\beta + C_{l_p}p\frac{b_{ref}}{2V_T} + C_{l_r}r\frac{b_{ref}}{2V_T} + C_{l_{\dot\beta}}\dot\beta\frac{b_{ref}}{2V_T} + C_{l_{\delta_a}}\delta_a + C_{l_{\delta_r}}\delta_r, \\
C_m &= C_{m_\alpha}\alpha + C_{m_q}q\frac{c_{ref}}{2V_T} + C_{m_{\dot\alpha}}\dot\alpha\frac{c_{ref}}{2V_T} + C_{m_{\delta_e}}\delta_e, \\
C_n &= C_{n_\beta}\beta + C_{n_p}p\frac{b_{ref}}{2V_T} + C_{n_r}r\frac{b_{ref}}{2V_T} + C_{n_{\dot\beta}}\dot\beta\frac{b_{ref}}{2V_T} + C_{n_{\delta_a}}\delta_a + C_{n_{\delta_r}}\delta_r,
\end{aligned}
\tag{20}
$$

where

$$
\begin{aligned}
\delta_e &= \frac{e_1 + e_2}{2}, \\
\delta_a &= \frac{a_1 - a_2}{2}, \\
\delta_r &= \frac{r_1 + r_2}{2},
\end{aligned}
\tag{21}
$$

where these symbols are specified in Table 1. These set of equations prescribe the non-dimensional coefficients in Equations (16) and (17) as a a function of the state. In the context of this paper, the control surface deflections are related to the control inputs by $u_1 = e_1$, $u_2 = e_2$, $u_3 = a_1$, $u_4 = a_2$, $u_5 = r_1$, and $u_6 = r_2$. Overall, the aircraft dynamics is given by the equations above along with an aerodynamic model. Such a model The model to be used herein is prescribed subsequently.

We can compactly describe the overall nonlinear model as

$$
\dot X = F(X, \Lambda U)
\tag{22}
$$

where the input U consists of u_i, for $i = 1, ..6$, and Λ is the control effectiveness matrix.

For control purposes, the nonlinear plant is linearized about a trim point (X_0, U_0) satisfying $F(X_0, U_0) = 0$. This leads to the linear time invariant system

$$
\dot x_p = A_p x_p + B_p u + g(x_p, u)
\tag{23}
$$

7

where

$$A_p = \left.\frac{\partial F(X,U)}{\partial X}\right|_{x_0,\,u_0}, \quad B_p = \left.\frac{\partial F(X,U)}{\partial U}\right|_{x_0,\,u_0}, \tag{24}$$

and $g(x_p, u)$ represents higher order terms.

2.2 Adverse Conditions

We now describe the three categories of upsets, damage, and failures that we shall introduce in the above model.

Flight upsets: These adverse conditions result from large deviations in the initial conditions of the state from the trim point at which the plant is derived. In this paper, such deviations will be called flight upsets regardless of their size. If a linear system is input-output stable, guarantees for a bounded state are automatically obtained. In practical situations the closed-loop system is subject to unknown bounded disturbances, case in which only uniform ultimate boundedness for linear plants has been proved. This implies that there are initial conditions for which the state may grow unbounded. Whether the actual responses are bounded and actually stay within acceptable limits needs to be demonstrated. In this paper, the initial condition of α will be considered uncertain. Since the baseline controller designed for the GTM does not enable lateral command following, flight upsets in $\beta(0)$ are omitted.

CG movement: A serious condition that needs to be addressed is structural damage. This causes, among other things, a movement of the CG from its nominal position. Changes to the moments in Equation (17) in a post-failure state are given by

$$\begin{bmatrix} \Delta L \\ \Delta M \\ \Delta N \end{bmatrix} = \begin{bmatrix} \Delta x \\ \Delta y \\ \Delta z \end{bmatrix} \times \bar{q}S \begin{bmatrix} \cos\alpha & 0 & -\sin\alpha \\ 0 & 1 & 0 \\ \sin\alpha & 0 & \cos\alpha \end{bmatrix} \begin{bmatrix} -C_D\cos\beta \\ C_Y \\ -C_L \end{bmatrix}, \tag{25}$$

where $[\Delta x, \Delta y, \Delta z]$ is the position vector of the actual CG location from the reference point in body axes. The contribution of the tangential component of the acceleration can be accounted for by using the inertia tensor about the actual CG, which is related to the nominal CG by

$$I_{CG} = I_{nominal} - m \begin{bmatrix} \Delta y^2 + \Delta z^2 & \Delta x\Delta y & \Delta x\Delta z \\ \Delta x\Delta y & \Delta x^2 + \Delta z^2 & \Delta y\Delta z \\ \Delta x\Delta z & \Delta y\Delta z & \Delta x^2 + \Delta y^2 \end{bmatrix} \tag{26}$$

In the studies that follow the contribution of the centripetal component of the acceleration resulting from CG movement is ignored. The reader can refer to [7] for an explicit formulation of the equations of motion.

8

Actuator Failures: We now consider adverse conditions that result from loss of control effectiveness and time delay.

As in reference [12], we model these failures by pre-multiplying the B_p matrix of the linearized model by the control effectiveness matrix Λ. That is, the B_p matrix in (23) is changed to $B_p\Lambda$ where Λ is a matrix of dimension 6×6, which is equal to the identity matrix in the nominal case. Loss of control effectiveness is modeled by making the terms in the diagonal of Λ less than one. For example, if the right elevator fails by 50%, and the left aileron fails by 40%, Λ takes on the form

$$\Lambda = \mathrm{diag}\left[1, 0.5, 0.6, 1, 1, 1\right].$$

In general, the control effectiveness matrix takes the form

$$\Lambda = \mathrm{diag}\left[\lambda_{e1}, \lambda_{e2}, \lambda_{a1}, \lambda_{a2}, \lambda_{r1}, \lambda_{r2}\right], \tag{27}$$

where $0 \leq \max\{\Lambda\} \leq 1$.

In addition to these actuator failures we will also consider time delay in all six control inputs and control surface lock-ups. In the latter type of failure, the duration of the lock-in-place failure will be consider an uncertain parameter. Note that from all uncertainties mentioned above, only those in Λ affect the value of the control U_0 at trim.

3 Adaptive Control Architecture

The proposed control architecture augments a nominal controller with an adaptive component. While the nominal controller is designed to meet the performance requirements under ideal operating conditions, the adaptive one copes with failures and uncertainties. The very same structure of the controller that was designed at Langley Research Center for the GTM will be used in the nominal controller. Details on such a structure are presented next.

3.1 Nominal Controller

The nominal controller has three main components, an array of low-pass and wash-out and filters, an LQR controller with integral action, and a hard-limiter to cope with control saturation. This limiter enforces an anti-integration wind-up logic based on the elevator deflection. This logic makes the system non-linear and time varying. Each of these components is described in more detail next.

3.1.1 Washout Filters and Low-pass Filters

The GTM model has an array of low-pass and wash-out and filters to mitigate measurement noise and improve handling qualities. A block diagram of the

system is shown in Figure 1. In particular, the states α, p, q, and r will be low-pass filtered but only p, q, and r will be washed-out. These filters will be taken into account when designing the nominal controller.
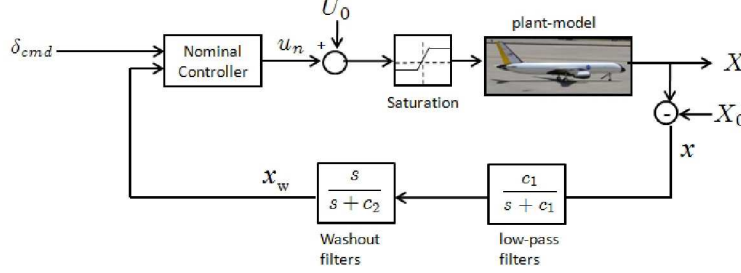

Figure 1. Washout filters and low-pass filters

3.1.2 LQR Controller with Integral Action

For control design purposes, we assume that the pitch, yaw and roll dynamics are weakly coupled. In order to closely follow a command in angle of attack, an integral state e_α is added

$$e_\alpha = \int(\alpha - \alpha_{\text{cmd}})dt \tag{28}$$

where $\alpha_{\text{cmd}} = 10\delta_{\text{e,cmd}}$ for $0 \leq \delta_{\text{e,cmd}} \leq 1$. Note that elevator command does not affect elevator angle, instead it generates integral error. The signal $\delta_{\text{e,cmd}}$ is one of the plant inputs in $\delta_{\text{cmd}} = \begin{bmatrix} \delta_{\text{e,cmd}}, \delta_{\text{a,cmd}}, \delta_{\text{r,cmd}} \end{bmatrix}^T$. The augmented plant dynamics is therefore described as

$$\underbrace{\begin{bmatrix} \dot{x}_p \\ \dot{e}_\alpha \end{bmatrix}}_{\dot{x}} = \underbrace{\begin{bmatrix} A_p & 0 \\ H & 0 \end{bmatrix}}_{A} \underbrace{\begin{bmatrix} x_p \\ e_\alpha \end{bmatrix}}_{x} + \underbrace{\begin{bmatrix} B_p \\ 0 \end{bmatrix}}_{B_1} u + \underbrace{\begin{bmatrix} 0 \\ -1 \end{bmatrix}}_{B_2} \alpha_{\text{cmd}} \tag{29}$$

Since the states in Equation (29) are accessible, an LQR controller is designed as

$$\delta_{e,n} = -\begin{bmatrix} K_{\delta_{e_\alpha}} & K_{\delta_{e_q}} & K_{\delta_{e_e}} \end{bmatrix} \begin{bmatrix} \alpha \\ q \\ e_\alpha \end{bmatrix}$$

$$\begin{bmatrix} \delta_{a,n} \\ \delta_{r,n} \end{bmatrix} = -\begin{bmatrix} K_{\delta_{a_p}} & K_{\delta_{a_r}} \\ K_{\delta_{r_p}} & K_{\delta_{r_r}} \end{bmatrix} \begin{bmatrix} p \\ r \end{bmatrix} + \underbrace{\begin{bmatrix} \delta_{a,cmd} \\ \delta_{r,cmd} \end{bmatrix}}_{K_r \delta_{\text{cmd}}} \tag{30}$$

where the control gains K_δ minimize the cost function

$$J = \int(x^T R_{xx} x + u^T R_{uu} u)dt, \tag{31}$$

10

and R_{xx}, R_{uu} are weighting matrices. As in the Langley controller, the gains $K_{\delta_{ar}}$ and $K_{\delta_{rp}}$ of the stability augmentation system in (30) are set to zero to eliminate coupling between the lateral and directional dynamics. When only the baseline controller is used $u = u_n = [\delta_{e,n}, \delta_{a,n}, \delta_{r,n}]$ and that $e_1 = e_2 = \delta_{e,n}/2$, $a_1 = -a_2 = \delta_{a,n}/2$ and $r_1 = r_2 = \delta_{r,n}/2$. Equations (28)-(30) describe the 6 DOF closed-loop dynamics of an LTI approximation of the GTM for an LQR controller with integral action.

3.2   Saturation

To ensure that the control input does not exceed the saturation limits for the three control surfaces, the rectangular saturation function

$$R_s(u_i) = \begin{cases} u_i & \text{if } |u_i| \leq u_{i,max}, \\ u_{i,max} \text{ sign}(u_i) & \text{if } |u_i| > u_{i,max}, \end{cases} \tag{32}$$

is used. The control deficiency caused by saturation is given by

$$u_\Delta = u - R_s(u). \tag{33}$$

Besides this physical saturation constraint, an anti-windup logic that depends on e_α is also implemented. This logic is governed by the time-varying saturation function

$$R_e(e_\alpha, \delta_e(t)) = \begin{cases} e_\alpha & \text{if } \dot{e}_\alpha \geq 0 \text{ or } e_\alpha \leq e_{\text{available}}, \\ e_{\text{available}} & \text{if } \dot{e}_\alpha < 0 \text{ and } e_\alpha > e_{\text{available}}. \end{cases} \tag{34}$$

where $e_{\text{available}}$ is given by

$$e_{\text{available}} = \max\left\{ 0, \frac{R_s(\delta_e) - (\delta_{e,\text{trim}} + K_{\delta_{e_\alpha}}\alpha + K_{\delta_{e_q}}q_w)}{K_{\delta_{e_\alpha}}} \right\}. \tag{35}$$

The error deficiency caused by the saturation function in Equation (34) is defined as

$$e_{\alpha,\Delta} = e_\alpha - R_e(e_\alpha, \delta_e(t)). \tag{36}$$

By replacing u with $R_s(u_n)$, and e_α with $R_e(e_\alpha, \delta_e(t))$ in Equation (29) we obtain the linear time varying system

$$\underbrace{\begin{bmatrix} \dot{x}_p \\ \dot{e}_\alpha \end{bmatrix}}_{\dot{x}} = \underbrace{\begin{bmatrix} A_p - B_p K_{x_p} & -B_p K_{\delta_{e_\alpha}} \\ H & 0 \end{bmatrix}}_{A_m} \underbrace{\begin{bmatrix} x_p \\ e_\alpha \end{bmatrix}}_{x} + \underbrace{\begin{bmatrix} B_p \\ 0 \end{bmatrix}}_{B_1} K_r \delta_{cmd}$$

$$+ \underbrace{\begin{bmatrix} 0 \\ -1 \end{bmatrix}}_{B_2} \alpha_{cmd} - \underbrace{\begin{bmatrix} B_p \\ 0 \end{bmatrix}}_{R_1} u_\Delta - \underbrace{\begin{bmatrix} -B_p K_{\delta_{e_\alpha}} \\ 0 \end{bmatrix}}_{R_2} e_{\alpha,\Delta}, \tag{37}$$

11

which is the closed-loop system corresponding to the nominal controller. The boundedness of this system can be established for all initial conditions inside a bounded set. This set extends to the entire state-space when the open-loop plant is stable and there is no unmodeled dynamics, e.g., no time-delay.

3.3 Adaptive Controller

Since the nominal controller in (30) has been designed for a plant-model under nominal conditions, it may prove to be inadequate in the face of failures and uncertainties. To compensate for this we augment the controller in (30) with an adaptive component as follows:

$$u = U_0 + u_n + u_a = U_0 + (K + \theta_x)x + (K_r + \theta_r)r + \hat{f} \tag{38}$$

where K and K_r are the feedback and feedforward gains of the baseline controller, while θ_x, θ_r, and $\hat{f}$ are adaptively adjusted to minimize the state error between the controlled plant-model and a reference model. $\hat{f}$ is chosen to generate the desired plant output for the commanded input. In the current problem, the reference model is prescribed by the non-linear closed-loop system corresponding to the baseline controller for the case where there are no uncertainties. None of the saturation functions above are included in the reference model. Figure 2 shows the block diagram of this control architecture. Adaptive controllers for the GTM using a reference model that accounts for
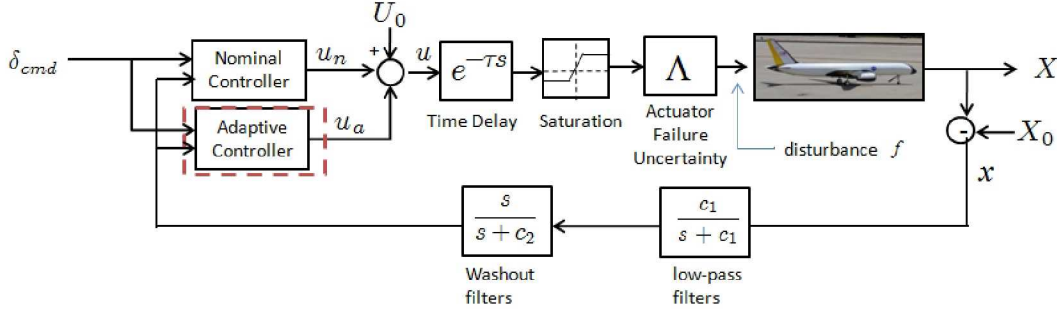
Figure 2. Control Architecture.

the time delay in telemetry have shown promise. Such controllers, however, will be presented in future publications.

Let the reference model be prescribed by $\dot{x}_m = f(x_m, u)$, where x_m is the reference model state. Linearization of this model about (X_0, U_0) leads to

$$\dot{x}_{ml} = A_m x_{ml} + B_m u + g(x_{ml}, u). \tag{39}$$

Defining the state error e as

$$e = x - x_m \tag{40}$$

12

we choose the adaptive laws [1] for adjusting the adaptive parameters in (38) as

$$\dot{\theta}_x = -\Gamma_1 B^T P e_u x^T - \sigma_1 \theta_x$$
$$\dot{\theta}_r = -\Gamma_2 B^T P e_u r - \sigma_2 \theta_r$$
$$\dot{\hat{f}} = -\Gamma_3 B^T P e_u - \sigma_3 \theta_f \tag{41}$$
$$\dot{\hat{\lambda}} = -\Gamma_4 \mathrm{diag}(u_\Delta) B_p^T P e_u - \sigma_4 \hat{\lambda}$$

where $A_m^T P + P A_m = -Q$, $Q > 0$, Γ_i is diagonal and positive definite for $i = 1, ...4$, and $e_u = e - e_\Delta$. The auxiliary error e_Δ is defined as

$$\dot{e}_\Delta = A_m e_\Delta - R_1 \mathrm{diag}(\hat{\lambda}) u_\Delta. \tag{42}$$

Note that if the control does not saturate $u_\Delta = 0$, $e_\Delta \to 0$ and $e_u \to e$. e_Δ is the error that occurs due to saturation, and by subtracting it out from e, we obtain e_u which is the sum of the error due to uncertainties and the error due to $e_{\alpha,\Delta}$. The σ modifications prevent the drift of the adaptive parameters θ_x, θ_r, $\hat{f}$ and $\hat{\lambda}$ caused by disturbances. The term $\hat{f}$ is an adaptive parameter aimed at counteracting constant disturbances.

It should be noted that the stability and boundedness of the closed-loop augmented system has been proved in [3, 13, 14] when physical saturation constraints are present. However, the stability analysis for the anti-windup logic in Equation (34) remains to be established.

4   Control Verification

This section introduces a framework for evaluating the degradation in closed-loop performance caused by increasingly larger values of uncertainty. This is attained by determining the largest hyper-rectangular set in the uncertain parameter space for which a set of closed-loop requirements are satisfied by all set members. A brief introduction to the mathematical framework required to perform this study is presented next. References [8] and [15] cover this material in more detail.

4.1   Mathematical Framework

The parameters which specify the closed-loop system are grouped into two categories: uncertain parameters, which are denoted by the vector p, and the control design parameters, which are denoted by the vector d. While the plant model depends on p (e.g., aerodynamic coefficients, initial conditions, time delay, actuator failures), the controller depends on d (e.g., control gains). The *Nominal Parameter* value, denoted as $\bar{p}$, is the value that p assumes when

there is no failure/uncertainty. The value of d on the other hand is assumed to be available and will remain fixed.

Stability and performance requirements for the closed-loop system will be prescribed by the set of constraint functions, $g(p, d) < 0$. This vector inequality, and all others that follow, hold component wise. For a fixed d, the larger the region in p-space where $g < 0$, the more robust the controller. The *Failure Domain* corresponding to the controller with parameters d is given by[1]

$$\mathcal{F}(d) = \bigcup_{j=1}^{\dim(g)} \mathcal{F}^j(d). \tag{43}$$

$$\mathcal{F}^j(d) = \{p : g_j(p, d) \geq 0\}, \tag{44}$$

While Equation (44) describes the failure domain corresponding to the jth requirement, Equation (43) describes the failure domain for all requirements. The *Non-Failure Domain* is the complement set of the failure domain and will be denoted[2] as $C(\mathcal{F})$. The names "failure domain" and "non-failure domain" are used because in the failure domain at least one constraint is violated while, in the non-failure domain, all constraints are satisfied.

Let Ω be a set in p-space, called the *Reference Set*, whose geometric center is the nominal parameter $\bar{p}$. The geometry of Ω will be prescribed according to the relative levels of uncertainty in p. One possible choice for the reference set is the hyper-rectangle

$$\mathcal{R}(\bar{p}, n) = \{p : \bar{p} - n \leq p \leq \bar{p} + n\}. \tag{45}$$

where $n > 0$ is the vector of half-lengths. One of the tasks of interest is to assign a measure of robustness to a controller based on measuring how much the reference set can be deformed before intersecting the failure domain. The *Homothetic Deformation* of Ω with respect to the nominal parameter point $\bar{p}$ by a factor of $\alpha \geq 0$, is the set $\mathcal{H}(\Omega, \alpha) = \{\bar{p} + \alpha(p - \bar{p}) : p \in \Omega\}$. The factor of this deformation, α, is called the *Similitude Ratio*. While expansions are accomplished when $\alpha > 1$, contractions result when $0 \leq \alpha < 1$. Hereafter, deformations must be interpreted as homothetic expansions or contractions.

In what follows we assume that the controller d satisfies the requirements for the nominal plant, i.e., $g(\bar{p}, d) < 0$. Intuitively, one imagines that a homothet of the reference set is being deformed until its boundary touches the failure domain. Any point where the deforming set touches the failure domain is a *Critical Parameter Value* (CPV). The CPV, which will be denoted as $\tilde{p}$, might not be unique. The deformed set is called the *Maximal Set* (MS) and

---

[1]Throughout this paper, super-indices are used to denote a particular vector or set while sub-indices refer to vector components, e.g., p_i^j is the ith component of the vector p^j.

[2]The complement set operator will be denoted as $C(\cdot)$.

will be denoted as $\mathcal{M}$. The MS is the largest homothet of Ω that fits within $C(\mathcal{F})$. The *Critical Similitude Ratio* (CSR), denoted as $\tilde{\alpha}$, is the similitude ratio of that deformation. While the CSR is a non-dimensional number, the *Parametric Safety Margin* (PSM), denoted as ρ and defined later, is its dimensional equivalent. Both the CSR and the PSM quantify the size of the MS. Details on the implementation of these ideas are presented next.

The CPV corresponding to the deformation of $\Omega = \mathcal{R}(\bar{p}, n)$ for the jth requirement is given by

$$\tilde{p}^j = \underset{p}{\operatorname{argmin}} \left\{ \|p - \bar{p}\|_n^\infty : g_j(p, d) \geq 0, Ap \geq b \right\}, \tag{46}$$

where $\|x\|_n^\infty = \sup_i \{|x_i|/n_i\}$ is the n-scaled infinity norm. The last constraint in Equation (46) is used to exclude regions of the parameter space where plants are infeasible and uncertainty levels are unrealistic. The overall CPV is

$$\tilde{p} = \tilde{p}^k, \tag{47}$$

where

$$k = \underset{1 \leq j \leq \dim(g)}{\operatorname{argmin}} \left\{ \|\tilde{p}^j - \bar{p}\|_n^\infty \right\}. \tag{48}$$

The critical requirement, which is the one preventing a larger deformation, is $g_k < 0$. Once the CPV has been found, the MS is uniquely determined by

$$\mathcal{M}(d) = \mathcal{R}(\bar{p}, \tilde{\alpha} n). \tag{49}$$

where $\tilde{\alpha} = \|\tilde{p} - \bar{p}\|_n^\infty$. The *Rectangular PSM* is defined as

$$\rho = \tilde{\alpha} \|n\|, \tag{50}$$

The last two equations, which apply to the overall CPV, can be extended to individual CPVs, by using $\tilde{p}^j$ instead of $\tilde{p}$. Note that overall PSM is equal to the smallest individual PSM.

Because the CSR and the PSM measure the size of the MS, their values are proportional to the degree of robustness of the controller associated with d to uncertainty in p. The CSR is non-dimensional, but depends on both the shape and the size of the reference set. The PSM has the same units as the uncertain parameters, and depends on the shape, but not the size, of the reference set. If the PSM is zero, the controller's robustness is practically nil since there are infinitely small perturbations of $\bar{p}$ leading to the violation of at least one of the requirements. If the PSM is positive, the requirements are satisfied for parameter points in the vicinity of the nominal parameter point. The larger the PSM, the larger the Ω-shaped vicinity.

15

4.1.1 One-dimensional Case

In the case where $\dim\{p\} = 1$, the expressions for the CPVs, the PSM, and the MS are given by

$$\tilde{p}^j = \underset{p}{\mathrm{argmin}}\left\{|p - \bar{p}| : g_j(p, d) \geq 0, Ap \geq b\right\}, \tag{51}$$

$$\tilde{p} = \tilde{p}^k, \tag{52}$$

$$\rho = |\tilde{p}^k - \bar{p}|, \tag{53}$$

$$\mathcal{M}(d) = (\bar{p} - \rho, \bar{p} + \rho), \tag{54}$$

where

$$k = \underset{1 \leq j \leq \dim(g)}{\mathrm{argmin}}\left\{|\tilde{p}^j - \bar{p}|\right\}. \tag{55}$$

Figure 3 shows an sketch with relevant variables and sets. Note that the non-failure domain is given by the intersection of the individual non-failure domains. Besides, the overall CPV is the parameter value closest to the nominal point where at least one component of g is equal to zero. From the figure we see that $\tilde{p}^1 - \bar{p} < \bar{p} - \tilde{p}^2$ so $\tilde{p} = \tilde{p}^1$ and $k = 1$. By construction, all the points within the MS, which is centered about the nominal parameter point, satisfy the closed-loop requirements.
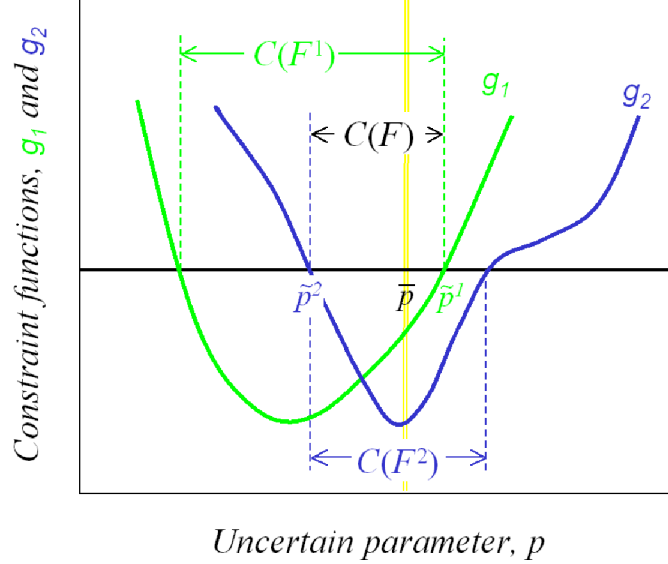
Figure 3. Relevant variables in a 1-dimensional p-space for a fixed d.

As expected, analyses arising from considering each uncertain parameter individually are unable to capture the effect of the dependencies among uncertain parameters. When such dependencies are important, the collection

16

of PSMs that result from performing dim(p) one-dimensional deformations can misrepresent the actual system's robustness. For instance, if ρ^1 is the PSM corresponding to a one-dimensional deformation in p_1, ρ^2 is the PSM corresponding to a one-dimensional deformation in p_2, and ρ^3 is the PSM corresponding to a two-dimensional deformation in $[p_1, p_2]$; it is possible to have $\rho^3 \ll \min\{\rho^1, \rho^2\}$. In such a case there is a combination of uncertain parameters much closer to $\bar{p}$ that will be missed by both one-dimensional searches.

4.2 Analysis Setup

4.2.1 Uncertain Parameters

We will consider the following set of uncertain parameters

$$[\Lambda_{\text{ele}}, \Lambda_{\text{ail}}, \Lambda_{\text{rud}}, \Lambda_{\text{thr}}, \tau, t_l, \Delta_x, \Delta_y, \Delta\alpha(0)], \tag{56}$$

where the first 6 components, can be categorized as actuator uncertainties or failures, the next two account for structural failures and last one for a flight upset. In particular,

$$\begin{aligned}
\Lambda_{\text{ele}} &= \begin{bmatrix} \lambda_{e1}, \lambda_{e2} \end{bmatrix} \\
\Lambda_{\text{ail}} &= \begin{bmatrix} \lambda_{a1}, \lambda_{a2} \end{bmatrix} \\
\Lambda_{\text{rud}} &= \begin{bmatrix} \lambda_{r1}, \lambda_{r2} \end{bmatrix} \\
\Lambda_{\text{thr}} &= \begin{bmatrix} \lambda_{t1}, \lambda_{t2}, \lambda_{t3}, \lambda_{t4} \end{bmatrix}
\end{aligned} \tag{57}$$

are the control effectiveness of elevators, ailerons, rudders, and engine throttle; τ is a time delay in all input channels, and t_l is the duration of a control surface lock-up. The terms Δ_x and Δ_y are components of the position vector in the xy-body frame of the post-failure CG location with respect to a reference point. The last component, which models a flight upset, is the initial condition in angle of attack. The nominal parameter values corresponding to the set of parameters in Equation (56) is $[1, 1, 1, 1, 0, 0, 0, 0, 0]$.

4.2.2 Closed-loop Requirements

The following stability and performance requirements will be considered

$$g_0 = \max\{[u_{trim} - u_{\max}, u_{\min} - u_{trim}]\}, \tag{58}$$

$$g_1 = \max_t \left\{ \frac{|\dot{V}_T|}{g} \right\} - 2.5, \tag{59}$$

$$g_2 = \left[(\alpha - \alpha_{\text{cmd}})^2 + k_\alpha \dot{\alpha}^2 + (\beta - \beta_{\text{cmd}})^2 + k_\beta \dot{\beta}^2 \right]_{t=t_f} - c_1, \tag{60}$$

$$g_3 = \eta(p, d) - c_2\eta(\bar{p}, d_{base}),$$
$$\eta = w_1||\alpha - \alpha_{\text{cmd}}||_2 + w_2||p - p_{\text{cmd}}||_2 + w_3||r - r_{\text{cmd}}||_2 \tag{61}$$

where $|| \cdot ||_2$ is the L_2 norm in the interval $[0, t_f]$. The first requirement, $g_0 < 0$, is used to determine if the vehicle has enough control authority to trim, i.e. if it satisfies $u_{min} < u_{trim} < u_{max}$. Note that this requirement is independent of d and may indicate instability. $g_1 < 0$ is a structural requirement enforced by preventing the loading factor from exceeding the upper limit of 2.5. The requirement $g_2 < 0$, where $0 < c_1 \ll 1$, $k_\alpha > 0$ and $k_\beta > 0$, enforces stability and satisfactory steady state performance. The last requirement, $g_3 < 0$, for $c_2 > 1$, $w_1 > 0$, $w_2 > 0$ and $w_3 > 0$, is used to measure satisfactory transient performance. This requirement prevents the cumulative error from exceeding a prescribed upper limit. Such a limit is c_2 times larger than the cumulative error incurred by the baseline controller under nominal flying conditions.

In practice, control requirements are prescribed in advance before the control design process even starts. When such requirements are only described qualitatively several implementations of the constraints g are possible. This creates the additional challenge of constructing functional forms that capture well the intent of the requirement while having a minimal amount of conservatism. This paper does not tackle such a challenge and assumes that the g above is given.

4.3 Flight Conditions (FC)

The closed-loop response depends on p and d as well as on the intended flight maneuver, denoted hereafter as f. This implies that $g(p, d, f)$. Two flight conditions, namely f_{lon} and f_{lat}, will be consider in the analyses that follow. In the former one, which mostly affects the longitudinal dynamics, a step input in δ_{ecmd} is commanded. In the second one, which affects both the longitudinal and lateral dynamics, the vehicle also starts from level flight and a set of commands in δ_{acmd} and δ_{rcmd} make the vehicle turn. Figures 4 and 5 show the vehicle's trajectory and relevant states for the longitudinal flight condition when there is no uncertainty/failure. The same information corresponding to the lateral flight condition is shown in Figures 6 and 7. The p command for f_{lat} is a sequence of two step inputs (only one is shown) where the second one cancels the first one after a suitable time.

5 Results

In this section, we evaluate the baseline controller in Equation (37) and the adaptive controller in Equations (38)- (42) according to the control verification setting of Section 4. The aerodynamic model used can be found in [9]. The numerical values of other variables are shown in Table 3.

Table 2. Cases analyzed

Case	Failure/Uncertainty	
Case A	Flight upset in angle of attack	$[\Delta\alpha(0)\ f_{\text{lon}}]$
Case B	CG movement along x-axis	$[\Delta_x\ f_{\text{lon}}]$
Case C	CG movement along y-axis	$[\Delta_y\ f_{\text{lat}}]$
Case D	Symmetric Aileron failure	$[\Lambda_{\text{ail}}\ f_{\text{lat}}]$
Case E	Symmetric Elevator failure	$[\Lambda_{\text{ele}}\ f_{\text{lon}}]$
Case F	Asymmetric Aileron failure	$[\lambda_{\text{a1}}\ f_{\text{lat}}]$
Case G	Asymmetric Throttle failure	$[\lambda_{\text{t1}}\ f_{\text{lon}}]$
Case H	Elevator lock-in-place failure	$[t_l\ f_{\text{lon}}]$
Case I	Time delay in all control inputs	$[\tau\ f_{\text{lon}}]$

Table 3. Numerical Values

Variable	Value
Velocity at trim	614(ft/sec)
Angle of Attack at trim	2.2(deg)
Height at trim	20000(ft)
$K_{\delta_{e_\alpha}}$	-0.4420
$K_{\delta_{e_q}}$	-0.9105
$K_{\delta_{e_e}}$	-0.7906
$K_{\delta_{a_p}}$	-0.1000
$K_{\delta_{r_r}}$	-0.3000
Γ_1	$\text{diag}([1,1,100,100,100,100]) \times 200$
Γ_2	$\text{diag}([1,1,100,100,100,100]) \times 100$
Γ_3	$\text{diag}([1,1,100,100,100,100]) \times 50$
Γ_4	$\text{diag}([1,1,1,1,1,1]) \times 100$
Q	$\text{diag}([1,1,1,1,1])$
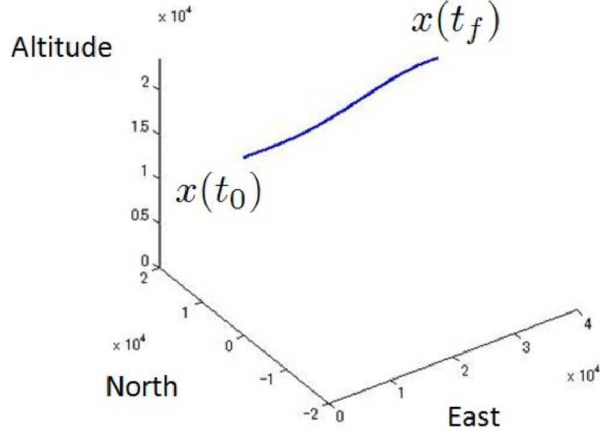
Figure 4. Trajectory associated with the longitudinal flight condition.
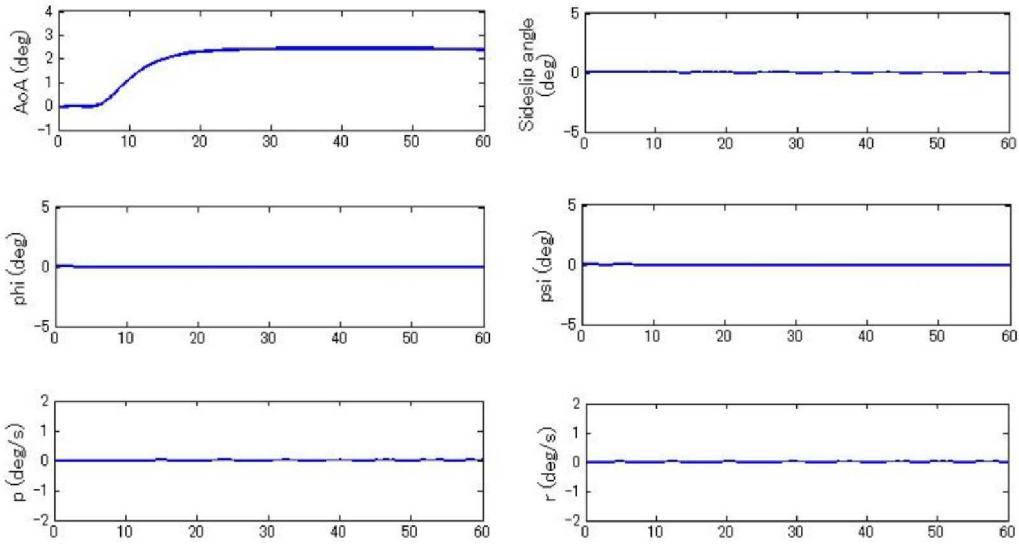
Figure 5. Relevant states for the longitudinal flight condition.

In Case A we consider a flight upset in the angle of attack, $\Delta\alpha(0)$ about $\alpha_{\text{trim}} = 2.20(\text{deg})$ for the longitudinal flight condition. The dependency of g on $\Delta\alpha(0)$ for both controllers is illustrated in Figure 8. The dashed lines and the solid lines represent results from the baseline and adaptive controllers respectively. A comparison of these curves shows that the non-failure region of the adaptive controller is larger by virtue of the structural and tracking performance requirements. The nominal parameter value is indicated as a
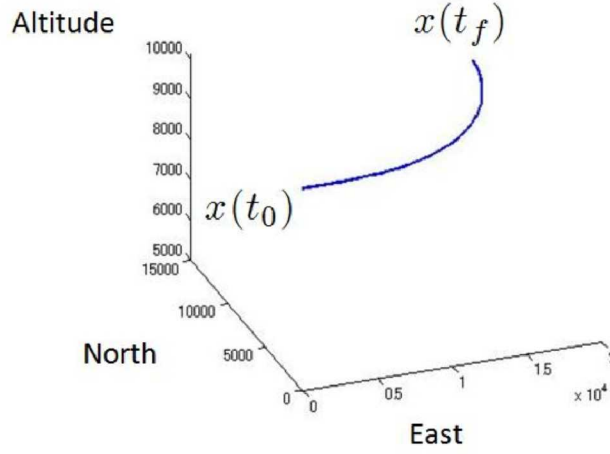
Figure 6. Trajectory associated with the lateral flight condition.
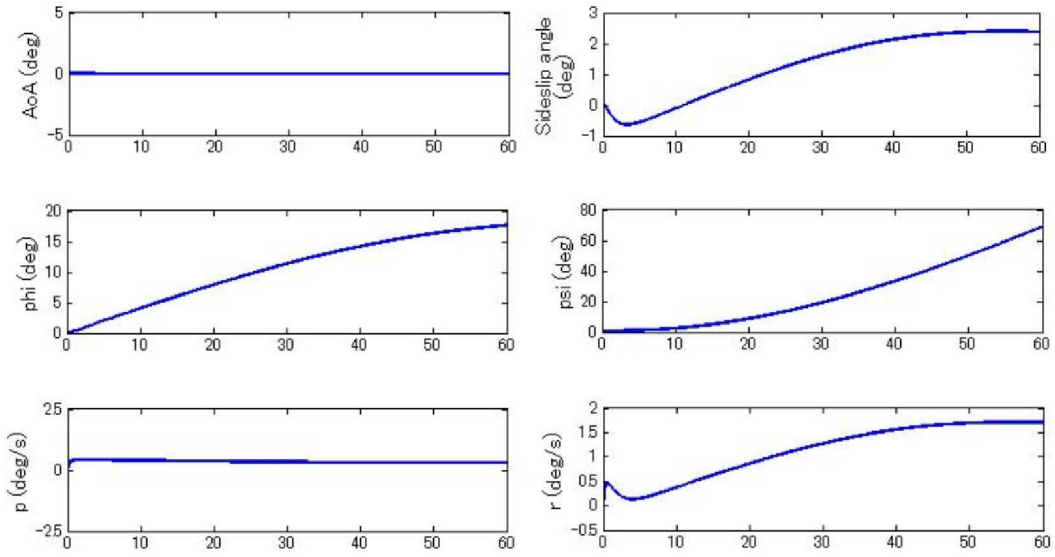
Figure 7. Relevant states for the lateral flight condition.

vertical yellow line. The line conventions used in this figure also apply to the figures that follow.

In Case B we consider the movement of the CG in the x-direction for the longitudinal flight condition. Recall that a positive value of the CG movement denotes a forward movement. Figure 9 illustrates the dependency of g on the CG location for both controllers. Note that the system loses stability when the CG moves backward, while the tracking performance degrades the faster

21
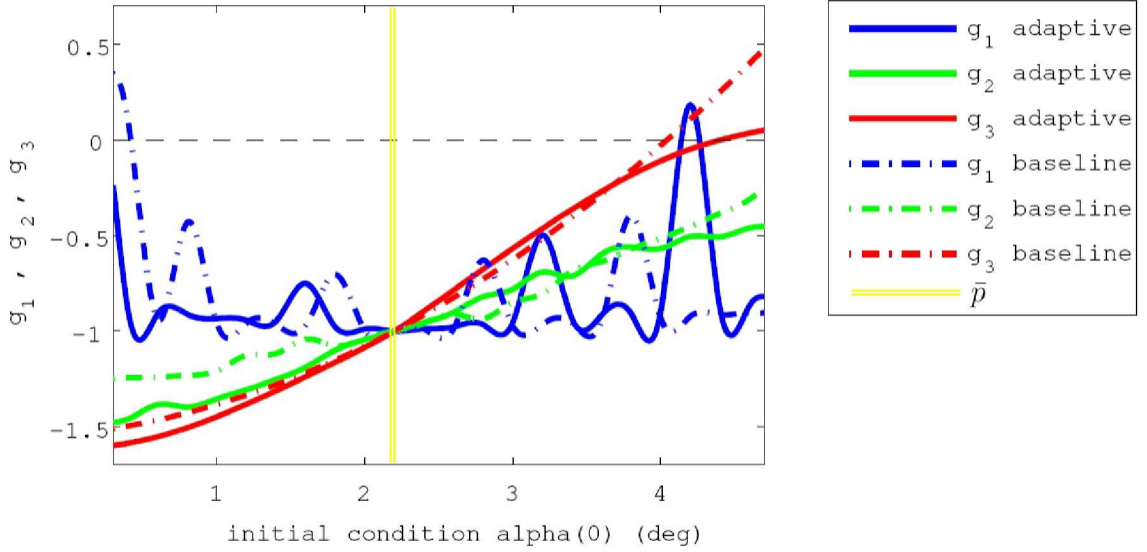
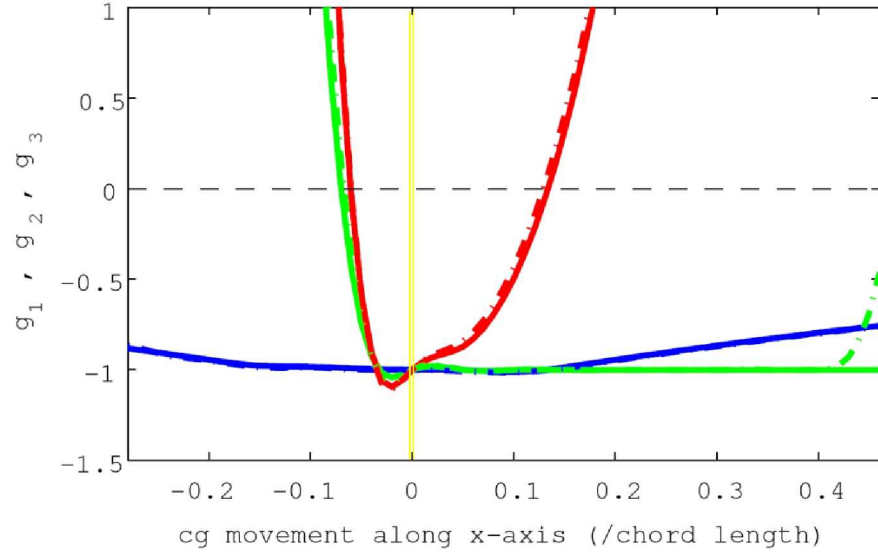Figure 8. Case A: $g(\alpha(0))$ for the longitudinal FC. Line convention: nominal parameter point (yellow), loading factor requirement (blue), steady-state requirement (green), tracking performance (red), adaptive controller (solid), baseline controller (dash-dot).

when the CG moves forward. The baseline controller has a PSM of 0.175 while the adaptive one attains a PSM of 0.197.

In Case C we consider the movement of the CG in the y-direction for the lateral flight condition. In this setting a positive CG movement denotes movement to the right. Figure 10 illustrates the dependency of g on the CG location for both controllers. The curves are asymmetric with respect to the nominal parameter value, since the flight condition is itself asymmetric. As before, the adaptive controller attains a larger PSM. The baseline controller has a PSM of 0.0029 while the adaptive one attains a PSM of 0.0069.

In Case D, we consider a symmetric failure in both ailerons, where $\lambda_{ail} = \lambda_{a_1} = \lambda_{a_2}$, for the lateral FC. Figure 11 illustrates the dependency of g on λ_{ail} for both controllers. While the PSM for the baseline is 6.6%, the PSM for the adaptive is 10%. In both cases, the tracking performance is the critical requirement.

In Case E we consider a symmetric failure in both elevators, where $\lambda_{ele} = \lambda_{e_1} = \lambda_{e_2}$, for the longitudinal FC. Figure 12 illustrates the dependency of g on λ_{ele} for both controllers. While the PSM for the baseline is 33%, the PSM for the adaptive is 42%. In both cases, the tracking performance is the critical requirement. As before, the adaptive controller has better robustness characteristics.

22

Figure 9. Case B: $g(\Delta_x/c_{ref})$ for the longitudinal FC. Line convention: nominal parameter point (yellow), loading factor requirement (blue), steady-state requirement (green), tracking performance (red), adaptive controller (solid), baseline controller (dash-dot).
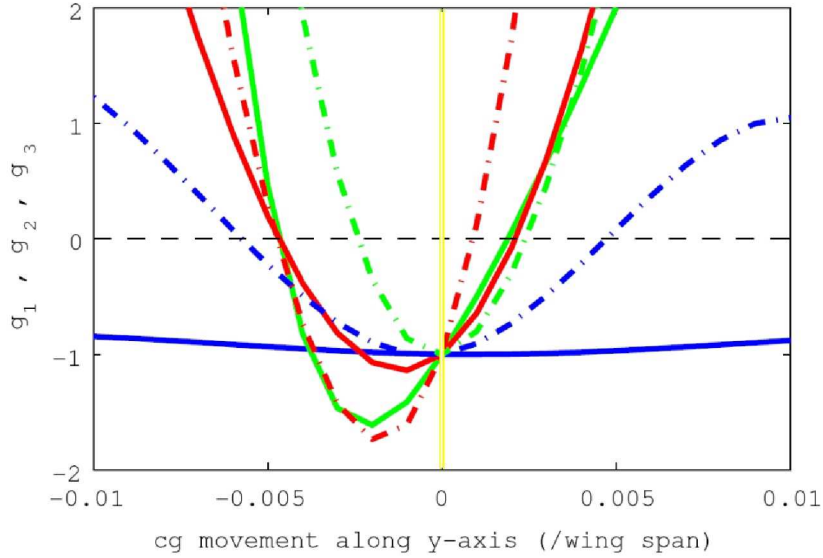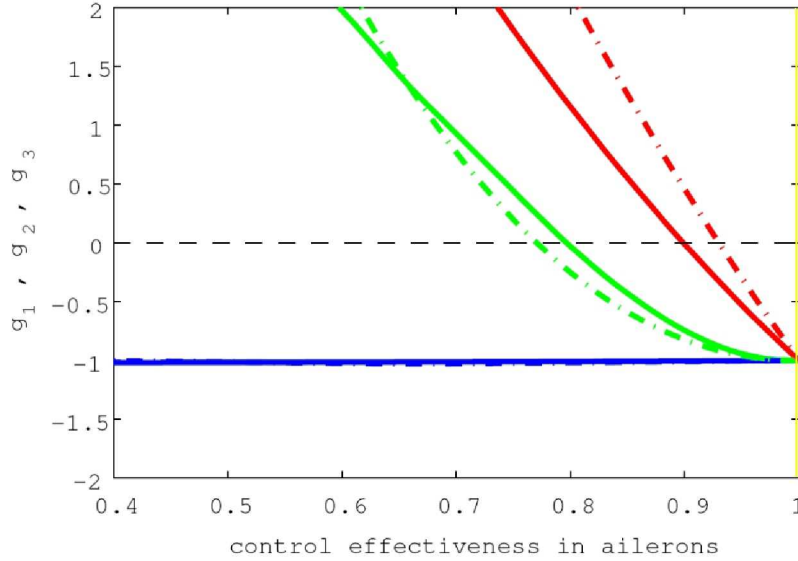

Figure 10. Case C: $g(\Delta_y/b_{ref})$ for the lateral FC. Line convention: nominal parameter point (yellow), loading factor requirement (blue), steady-state requirement (green), tracking performance (red), adaptive controller (solid), baseline controller (dash-dot).

23

Unlike Case C, Case F considers an asymmetric aileron failure where λ_{a_1} is uncertain and $\lambda_{a_2} = 1$. Figure 13 illustrates the dependency of g on λ_{a_1} for both controllers. While the PSM for the baseline is 14%, the PSM for the adaptive is 20%. Consistently, the tracking performance requirement remains as a critical requirement. Note however, that the PSM corresponding to the stability requirement for the adaptive controller becomes smaller.

Figure 11. Case D: $g(\Lambda_{ail})$ for the lateral FC. Line convention: nominal parameter point (yellow), loading factor requirement (blue), steady-state requirement (green), tracking performance (red), adaptive controller (solid), baseline controller (dash-dot).

In Case G we consider a failure in the left outboard engine λ_{t1} for the longitudinal FC. Figure 14 illustrates the dependency of g on λ_{t1} for both controllers. While the PSM for the baseline is 1.7%, the PSM for the adaptive is 2.9%. As before, the tracking performance is the critical requirement. Note that the margins obtained in this case are considerably smaller than those found in the other cases. The non-failure domains are small since the throttle inputs are not controlled and remain fixed at their trim values. A time simulation for a 40% loss in control effectiveness occuring 7s after the step input has been commanded is shown in Figure 15. Note that this point belongs to the $C(\mathcal{F}^2)$ corresponding to the adaptive controller and to the $\mathcal{F}^2$ corresponding to the baseline. Results similar to those in Figure 14 were observed when the Lateral FC was used.

A lock-in-place failure in the left elevator is considered in Case H. This is simulated by keeping this control input at a constant value for a period of t_l
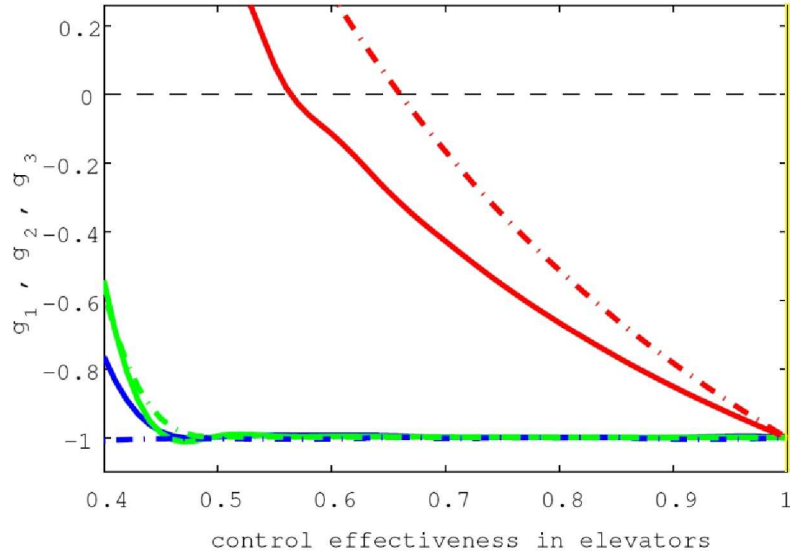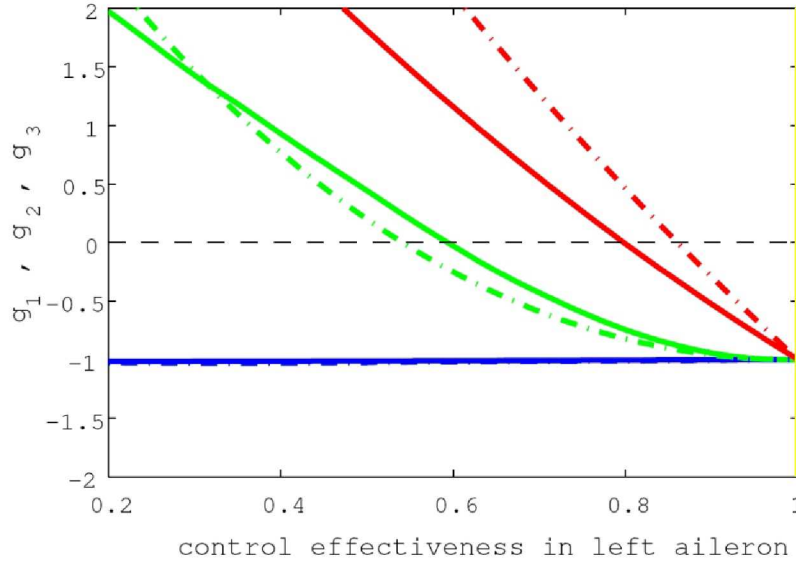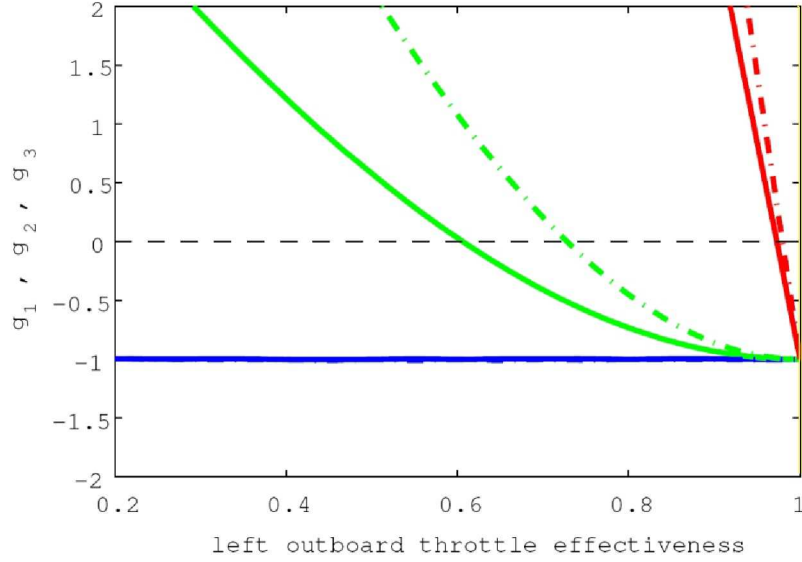
Figure 12. Case E: $g(\Lambda_{ele})$ for the longitudinal FC. Line convention: nominal parameter point (yellow), loading factor requirement (blue), steady-state requirement (green), tracking performance (red), adaptive controller (solid), baseline controller (dash-dot).
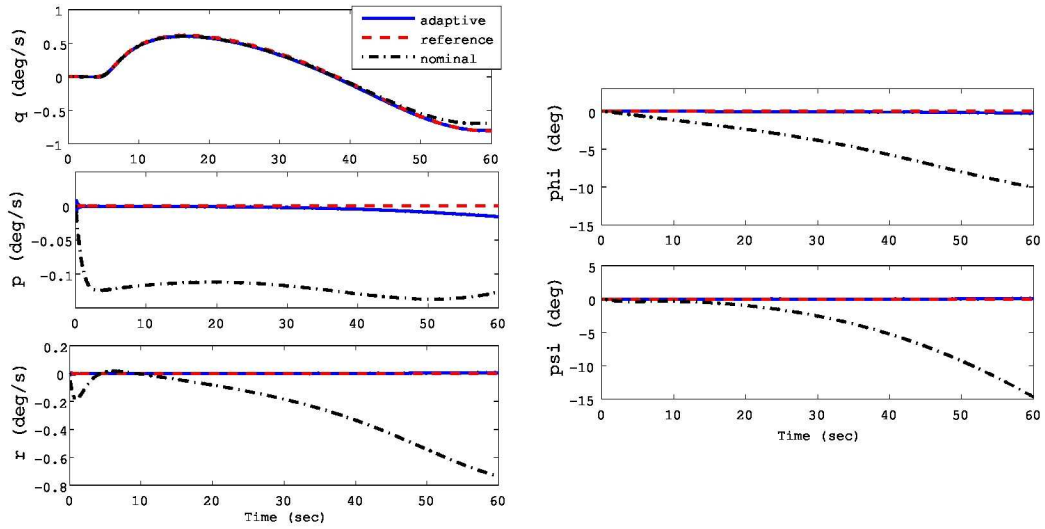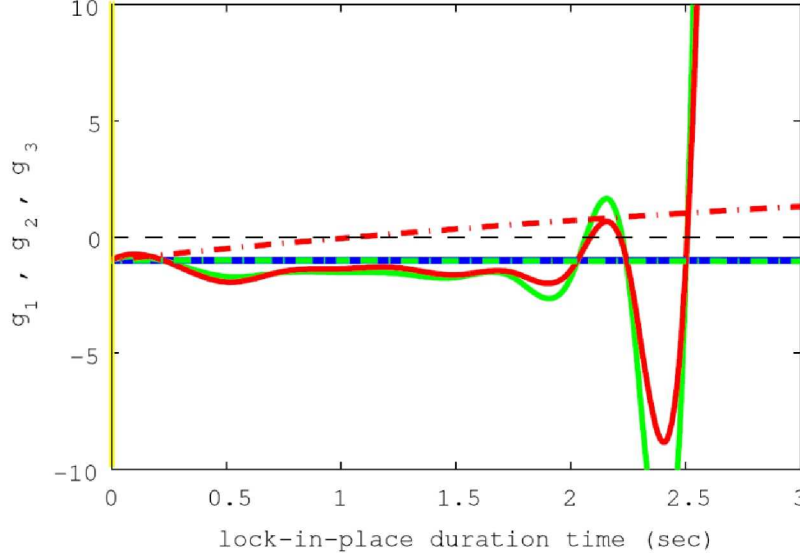

Figure 13. Case F: $g(\lambda_{a_1})$ for the lateral FC. Line convention: nominal parameter point (yellow), loading factor requirement (blue), steady-state requirement (green), tracking performance (red), adaptive controller (solid), baseline controller (dash-dot).

Figure 14. Case G: $g(\lambda_{t1})$ for the longitudinal FC. Line convention: nominal parameter point (yellow), loading factor requirement (blue), steady-state requirement (green), tracking performance (red), adaptive controller (solid), baseline controller (dash-dot).

Figure 15. Time simulation for $\lambda_{t1} = 0.6$.

seconds. The larger the t_l the most severe the failure, being ∞ the practical case of interest. Figure 16 illustrates the dependency of g on the lock-in time. Substantial differences in the functional dependencies are apparent. It can be seen that the PSM for the baseline is 1.1 while the PSM for the adaptive is 2.1. Note also that while the tracking performance is critical for the baseline controller, the stability requirement is critical for the adaptive one. Case I

Figure 16. Case H: $g(t_l)$ for the longitudinal FC. Line convention: nominal parameter point (yellow), loading factor requirement (blue), steady-state requirement (green), tracking performance (red), adaptive controller (solid), baseline controller (dash-dot).

considers the case when there is a time delay τ in all three control inputs. Figure 17 illustrates the dependency of g on this uncertain parameter for the longitudinal flight condition. In contrast to all other cases, the non-failure domain of the adaptive controller is smaller that that of the baseline. Hence, the nominal controller is more robust to time delay than the adaptive one. One may infer that this is the price of attaining improved system performance through aggressive actuation. Note however, that this observation may not hold when multiple uncertainties occur simultaneously. Figure 18 shows time responses for both controllers when $\tau = 0.74$s. This point belongs to the non-failure domain of the baseline controller and to the failure domain of the adaptive one.

Table 4 summarizes the results above by presenting the relative change in PSM attained by the adaptive controller and the critical requirement. In all
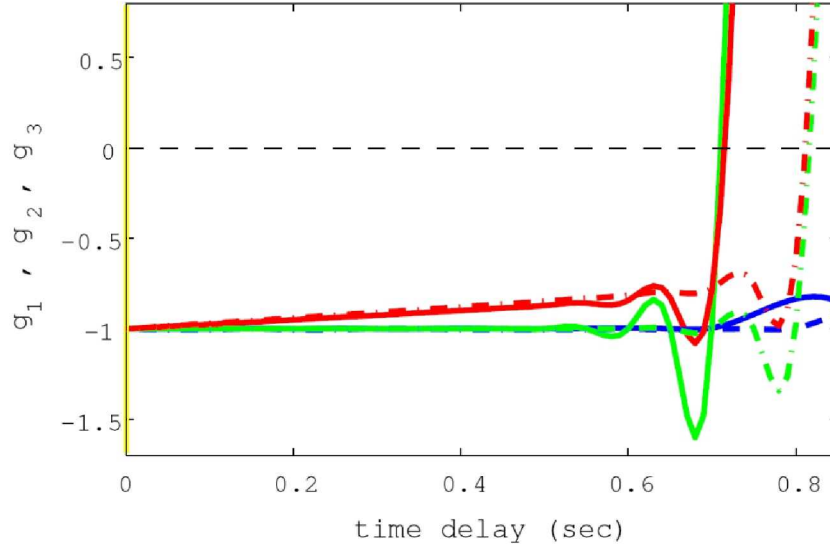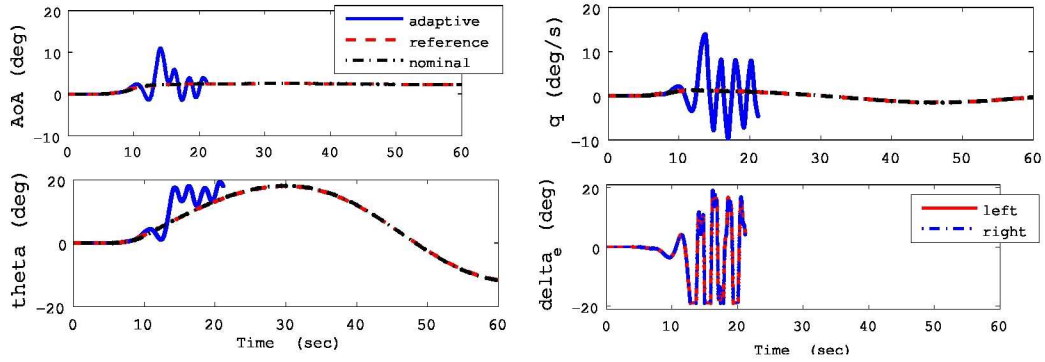
Figure 17. Case I: $g(\tau)$ for the longitudinal FC. Line convention: nominal parameter point (yellow), loading factor requirement (blue), steady-state requirement (green), tracking performance (red), adaptive controller (solid), baseline controller (dash-dot).

Figure 18. Time simulation for $\tau = 0.74$s.

Table 4. Summary of results

Case	$\left(\frac{\rho_{adap}}{\rho_{base}} - 1\right) \times 100\%$	Critical Requirement
A	+4.01 %	g_1, g_3
B	+11.4 %	g_2, g_3
C	+133 %	g_2, g_3
D	+63.6 %	g_3
E	+27.3%	g_3
F	+46.7 %	g_3
G	+70.6 %	g_3
H	+88.9 %	g_2, g_3
I	-13.9 %	g_2, g_3

but one of the cases cases, the adaptive controller attains better robustness by a sizable margin.

5.1 Multi-dimensional Case

In all the cases above a single uncertain parameter has been considered. In this setting, the effect of the dependencies among parameters cannot be captured. The same analysis can be conducted for a multi-dimensional vector p. In such a case, multiple failures and uncertainties occur simultaneously and the correlation among them may play a significant role. Studies of this type will be presented in the future. However, Figure 19 presents a time simulation of the controlled response for a multi-dimensional parameter realization when 2 pitch rate doublets are commanded. Therein, we assume loss in control effectiveness of 30% for the elevators, 10% for the ailerons, and 10% for the rudders. In addition, the CG has been moved to the left by $0.004b_{ref}$, and an initial condition in the angle of attack of 0.2 degrees is assumed. It is apparent that the adaptive controller achieves good tracking performance while the nominal controller cannot recover and makes the system unstable.
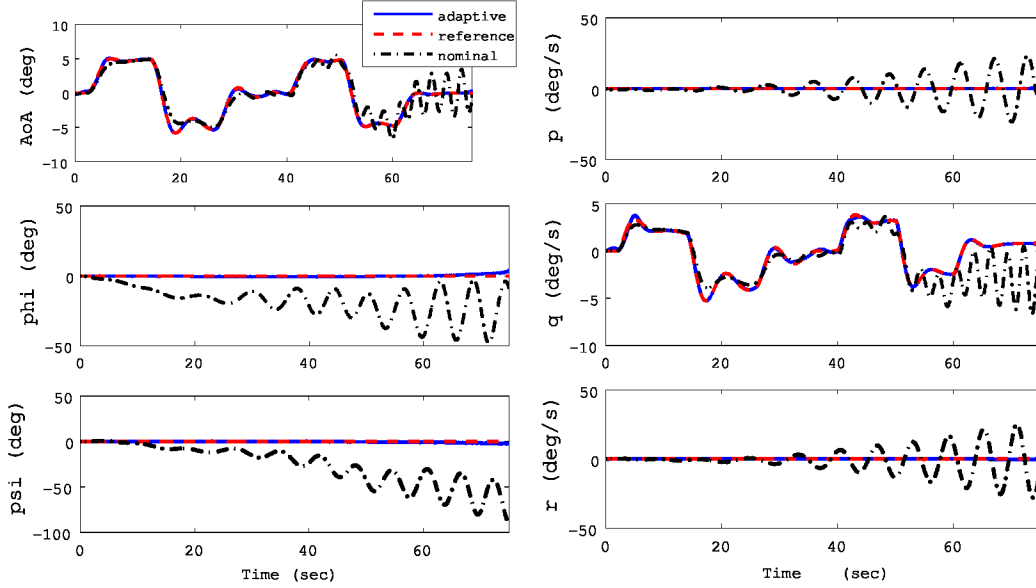

Figure 19. Time simulation for multiple uncertainties.

6 Conclusions

This paper presents an adaptive control architecture for safe flight of a transport aircraft under adverse operating conditions and uncertainties. This architecture combines a nominal controller based on an LQR with integral action, and an adaptive controller that accommodates actuator saturation and disturbances. The resilience of both controllers to uncertainty is studied using

a control verification methodology, where flight upsets, CG movements, and actuator failures are considered individually. The results of this study show that the adaptive controller enlarges the region of satisfactory performance by sizable margins in all cases but one. This exception was observed in the case of time-delay uncertainty, case for which the adaptive controller is less robust than the baseline controller. A more accurate robustness assessment will result from considering multiple uncertainties simultaneously. Such studies will indicate if the trends observed herein hold in a more realistic setting. Since the adaptive controller was not designed specifically for the uncertainties and closed-loop requirements used for its assessment, the improvements in robustness observed are particularly remarkable.

7 Acknowledgments

References

1. Narendra, Kumpati S.; and Annaswamy, Anuradha M.: *Stable Adaptive Systems*. Prentice-Hall, Englewood Cliffs, NJ, 1989.

2. Khalil, Hassan K.: *Nonlinear Systems*. Prentice-Hall, Upper Saddle River, NJ, 1996.

3. Karason, S. P.; and Annaswamy, A. M.: Adaptive Control in the Presence of Input Constraints. *IEEE Transaction on Automatic Control*, vol. 46, no. 11, November 1994, pp. 2325–2330.

4. Dydek, Zachary T.; Jain, Himani; Jang, Jinho; Annaswamy, A. M.; and Lavretsky, E.: Theoretically Verifiable Stability Margins for an Adaptive Controller. *Proc. AIAA Conference on Guidance, Navigation, and Control*, Keystone, Colorado, August 2006, AIAA-2006-6416.

5. Jang, Jinho; Annaswamy, A. M.; and Lavretsky, E.: Towards Verifiable Adaptive Flight Control in the Presence of Actuator Anomalies. *Proc. Conference on Decision and Control*, San Diego, California, December 2006, pp. 3300–3305.

6. Bailey, R. M.; Hostetler, R. W.; Barnes, K. N.; and Belcastro, C. M.: Experimental Validation: Subscal Aircraft Ground Facilities and Integrated

Test Capability. *AIAA Guidance, Navigation, and Control Conference*, 2005, AIAA-2005-6433.

7. Bacon, Barton J.; and Gregory, Irene M.: General Equations of Motion for a Damaged Asymmetric Aircraft. *AIAA Atmospheric Flight Mechanics Conference and Exhibit*, Hilton Head, South Carolina, August 2007, AIAA-2007-6306.

8. Crespo, L. G.; Giesy, D. P.; and Kenny, S. P.: Figures of Merit for Control Verification. *AIAA-2008-6339*, August 2008.

9. Heffley, Robert K.; and Jewell, Wayne F.: *Aircraft Handling Qualities Data*. Contractor's Report CR-2144, NASA, Systems Technology, Inc. Hawthorne, CA 90250, December 1972. Available at ntrs.nasa.gov.

10. Stevens, B.; and Lewis, F.: *Aircraft Control and Simulation, 2nd Edition*. Wiley-Interscience, Reston, 2003.

11. Nelson, R. C.: *Flight Stability and Automatic Control*. McGraw-Hill, 1989.

12. Jang, J; Annaswamy, A. M.; and Lavretsky, E.: Adaptive Flight Control in the Presence of Multiple Actuator Anomalies. *American Control Conference*, New York, NY, 2007, pp. 3300–3305.

13. Schwager, Mac; and Annaswamy, A. M.: Adaptive Control of Multi-Input Systems with Magnitude Saturation Constraints. *Proc. Conference on Decision and Control*, Seville, Spain, December 2005, pp. 783–788.

14. Jang, J.; Annaswamy, A. M.; and Lavretsky, E.: Adaptive Flight Control in the Presence of Multi-input Magnitude Saturation. *American Control Conference*, 2008.

15. Crespo, L. G.; Giesy, D. P.; and Kenny, S. P.: Robust Analysis and Robust Design of Uncertain Systems. *AIAA Journal*, vol. 46, no. 2, 2008.

REPORT DOCUMENTATION PAGE

1. REPORT DATE *(DD-MM-YYYY)*	2. REPORT TYPE	3. DATES COVERED *(From - To)*
01-02-2010	Contractor Report	

4. TITLE AND SUBTITLE

An Adaptive Control Technology for Safety of a GTM-like Aircraft

5a. CONTRACT NUMBER

NNX08AC62A

5b. GRANT NUMBER

5c. PROGRAM ELEMENT NUMBER

6. AUTHOR(S)

Matsutani, Megumi; Crespo, Luis G.; Annaswamy, Anuradha; Jang, Jinho

5d. PROJECT NUMBER

5e. TASK NUMBER

5f. WORK UNIT NUMBER

736466.11.01.07.43.17.01

7. PERFORMING ORGANIZATION NAME(S) AND ADDRESS(ES)

NASA Langley Research Center
Hampton, VA 23681-2199

8. PERFORMING ORGANIZATION REPORT NUMBER

9. SPONSORING/MONITORING AGENCY NAME(S) AND ADDRESS(ES)

National Aeronautics and Space Administration
Washington, DC 20546-0001

10. SPONSOR/MONITOR'S ACRONYM(S)

NASA

11. SPONSOR/MONITOR'S REPORT NUMBER(S)

NASA/CR-2010-216202

12. DISTRIBUTION/AVAILABILITY STATEMENT

Unclassified - Unlimited
Subject Category 08
Availability: NASA CASI (443) 757-5802

13. SUPPLEMENTARY NOTES

Langley Technical Monitor: Sean P. Kenny

14. ABSTRACT

An adaptive control architecture for safe performance of a transport aircraft subject to various adverse conditions is proposed and verified in this report. This architecture combines a nominal controller based on a Linear Quadratic Regulator with integral action, and an adaptive controller that accommodates actuator saturation and bounded disturbances. The effectiveness of the baseline controller and its adaptive augmentation are evaluated using a stand-alone control verification methodology. Case studies that pair individual parameter uncertainties with critical flight maneuvers are studied. The resilience of the controllers is determined by evaluating the degradation in closed-loop performance resulting from increasingly larger deviations in the uncertain parameters from their nominal values. Symmetric and asymmetric actuator failures, flight upsets, and center of gravity displacements, are some of the uncertainties considered.

15. SUBJECT TERMS

Adaptive control; Aviation safety; Control verification; GTM

16. SECURITY CLASSIFICATION OF:			17. LIMITATION OF ABSTRACT	18. NUMBER OF PAGES	19a. NAME OF RESPONSIBLE PERSON
a. REPORT	b. ABSTRACT	c. THIS PAGE			STI Help Desk (email: help@sti.nasa.gov)
U	U	U	UU	37	19b. TELEPHONE NUMBER *(Include area code)* (443) 757-5802